JOURNAL OF MATERIALS SCIENCE 19 (1984) 4068–4076

Thermal shock of ß-alumina with zirconia additions

J. R. G. EVANS, R. STEVENS
Department of Ceramics, Houldsworth School of Applied Science, University of Leeds, UK

S. R. TAN
Chloride Silent Power Ltd, Runcorn, Cheshire, UK

Sodium β-alumina electrolyte tubes were prepared from spray dried precursor powders with additions of 2, 5, 10 and 15 wt % ZrO_2 made by the sodium zirconate route. The thermal shock behaviour of ring segments cut from the tubes was examined by quenching into water at 0° C. At the 2% ZrO_2 level the dispersed ZrO_2 particle size was low, $<0.5\,\mu m$, and the tetragonal phase was retained. For higher weight fractions, particle coarsening during the β-alumina sintering schedule was extensive and the large particles transformed to monoclinic on cooling. At the 15% ZrO_2 level the β-alumina had a slightly reduced strength and high resistance to thermal shock and to thermal shock damage, quenching into water from 800° C effecting only a 43% reduction in strength. These observations are consistent with the effects of microcracking in the vicinity of second phase ZrO_2 particles.

1. Introduction

Sodium β-alumina is used as the electrolyte membrane in the sodium sulphur battery. Failure of the electrolyte tube remains a critical problem area in the development of this high energy/power density battery. Recent developments in the toughening of brittle materials by incorporating a dispersed second phase of transformable tetragonal zirconium oxide [1–3] have led to similar attempt to toughen β-alumina electrolytes [4, 5]. The present work describes initial experiments in which additions of ZrO_2 in the form of sodium zirconate were made to a magnesia and lithia stabilized β-alumina. The extent of thermal shock damage was investigated by measuring the reduction in strength of semicircular ring segments after quenching from various temperatures into water.

2. Experimental details

Sodium zirconate was synthesized by dry vibromilling stoichiometric proportions of ZrO_2* and Na_2CO_3 for 16 h followed by calcining at 1200° C for 2 h; subsequently a further dry vibromilling for 16 h took place. Conversion to Na_2ZrO_3 was confirmed using X-ray diffraction (XRD). The powders required to give a final composition of: 8.6 wt % Na_2O, 1 wt % MgO, 0.5 wt % Li_2O and X wt % ZrO_2 (where $X = 2, 5, 10, 15$) were spray dried and formed into tubes by isostatic pressing. After prefiring at 900° C to remove residual volatiles the tubes were sintered in a pilot plant zone sintering furnace at 1660° C (no ZrO_2), 1625° C (2, 5, 10 wt % ZrO_2) and 1610° C (15 wt % ZrO_2).

After fabrication the ZrO_2 content was assayed by X-ray fluorescence, and the actual ZrO_2 levels differed from the nominal amounts due to processing errors, particularly in the proportion of stoichiometric sodium zirconate.

Ring segments were cut from the tubes using a diamond impregnated saw, employing a low feed rate to minimize damage. Quenching was effected by equilibrating at a predetermined temperature in

*M.E.L. SC10.

0022–2461/84 $03.00 + .12

TABLE I Proportions of monoclinic zirconia by XRD

	Wt % monoclinic			
	2	5	10	15
As-sintered surface	9	80	88	89
1 μm diamond polish	12	71	84	87
Diamond ground surface	20	75	83	83
Powdered	19	77	86	87

TABLE II Density and porosity for β-alumina with ZrO_2 additions. $\rho_{tetr.} = 6100\,kg\,m^{-3}$, $\rho_{mono.} = 5560\,kg\,m^{-3}$

ZrO_2 addition		Density ($kg\,m^{-3}$)	Theoretical density ($kg\,m^{-3}$)	Porosity (%)
Nominal	Actual			
none	–	3240	3290	1.5
2%	1.65%	3259	3315	1.7
5%	3.71%	3315	3342	0.8
10%	9.91%	3405	3431	0.8
15%	12.4%	3423	3468	1.3

a vertical tube furnace with a release mechanism described previously [6]. The samples were contained in a stainless steel wire basket and released into water at 0° C. The rings were tested in compression and tension using a procedure previously described [7].

The fraction of tetragonal zirconia was deduced from XRD data using the monoclinic $(1\,1\,\bar{1})$ reflection and the tetragonal $(1\,1\,1)$ reflection and the empirical formula [8]:

$$\text{wt fraction tetragonal} = \frac{T_{(111)}}{T_{(111)} + 0.85M_{(11\bar{1})}}$$

where $T_{(111)}$ and $M_{(11\bar{1})}$ refer to peak areas measured by image analysis*. Samples which had been powdered were examined by diffractometry within 5 min of comminution to avoid interference by the sodium aluminate peak at 0.296 nm.

3. Results and discussion

3.1. XRD and thermal shock testing

X-ray diffraction was used to characterize the zirconia, making use of the $(1\,1\,1)$ tetragonal reflection and the $(1\,1\,\bar{1})$ monoclinic reflection, most other strong reflections for zirconia being obscured by the β-alumina peaks. The results in Table I show that for the samples containing 2% zirconia the weight fraction of the tetragonal phase is ~90% and furthermore that only ~10% of the available tetragonal is transformable on grinding. Subsequent examination using scanning electron microscopy (Fig. 7) shows that the particle size is $\leqslant 0.5\,\mu m$. Thus the surface energy and elastic constant of the matrix [5] are sufficient to stabilize the unalloyed zirconia and only a small fraction (0.2% of the ceramic) is available for toughening. In the material containing 5% by weight of zirconia, scanning electron microscopy reveals larger, ~4 μm, particles (Fig. 8) and XRD shows that these larger particles have transformed to monoclinic on cooling, leaving only ~20% tetragonal, 25% of which is capable of mechanically induced transformation to monoclinic on grinding. At the 15 wt % ZrO_2 level only ~10% tetragonal is retained and the availability of transformable tetragonal is negligible. ZrO_2 particles up to ~12 μm can be seen throughout the sample. This is consistent with the effect of particle size on the constrained transformation.

These results clearly demonstrate the importance of particle coarsening of zirconia added by the sodium zirconate route during the sintering schedule for β-alumina. It is probable that an Ostwald ripening process controls the scavenging of the finely divided ZrO_2 which is produced by deposition from sodium zirconate, and permits the production of large particles. It appears that as the overall fraction of ZrO_2 increases much larger particles can be produced from the greater quantity of local ultrafine ZrO_2. This ripening process may limit the usefulness of the sodium zirconate route for adding ZrO_2 to some ceramics.

Having established the phase composition of the zirconia and knowing the weight per cent addition it is possible to estimate the theoretical density and thus the porosity levels of samples from density determinations. Table II shows the density measured on small sections of tube by the water immersion method together with theoretical density calculated for the mixtures, taking the density of tetragonal zirconia as $6100\,kg\,m^{-3}$ and monoclinic as $5560\,kg\,mm^{-3}$ [10]. This shows that the density is consistently >98%, even with a reduced firing temperature for material with zirconia additions.

Initial strengths were measured on both internal and external surfaces of ring segment samples. The results in Table III indicate that there is a slight

* Kontron, W. Germany.

TABLE III Initial strength of zirconia toughened β-alumina

% ZrO_2	Tested after 2 weeks		Tested after 12 weeks
	External surface σ_f (MPa) ± S.D. (n)	Internal surface σ_f (MPa) ± S.D. (n)	External surface σ_f (MPa) ± S.D. (n)
0	192 ± 28 (20)	213 ± 27 (20)	–
2	193 ± 29 (6)	271 ± 55 (6)	255 ± 28 (4)
5	244 ± 14 (5)	278 ± 21 (5)	232 ± 30 (8)
10	216 ± 13 (4)	256 ± 14 (4)	243 ± 13 (4)
15	202 ± 8 (4)	238 ± 12 (4)	228 ± 3 (4)

fall in strength at the 15% ZrO_2 level. This is to be expected from the high monoclinic content and from the presence of microcracks as shown in Fig. 10. The latter were revealed by chemical etching of polished sections; these microcracks could not be observed on polished sections without chemical etching.

Table III also indicates that there is a slight increase in strength during storage. A possible cause for this phenomenon is that microcracks already present in the material are blunted by the ingress of moisture.

Optical microscopy on polished sections of as-fabricated electrolyte showed evidence of excessive β-alumina grain growth particularly in the 15% ZrO_2 material (Fig. 6). It is thought that zirconia acts as a "getter" for CaO impurities in the alumina which would otherwise inhibit grain growth.

The thermal shock behaviour of β-alumina with ZrO_2 additions is shown in Figs. 1 to 5 where the strength of semicircular ring segments is used as an indication of the degree of damage introduced by quenching the samples from a temperature, ΔT° C, into water at 0° C. For all the compositions used a clearly defined critical temperature ΔT_c for onset of damage was observed. ΔT_c can be related to the initial fracture strength, σ_i, all other factors being equal [11], and is a measure of the resistance to onset of damage, a useful parameter for the design engineer. A feature of the present work is that ΔT_c for the 15% ZrO_2 material was considerably raised to over 300° C (Table IV) without a corresponding increase in the initial fracture strength. Dilatometry did not yield significantly different values for the coefficient of thermal expansion. Thus a toughening process appears operative in thermal shock conditions which is not reflected in the room temperature modulus of rupture measurements at low strain rates.

The degree of damage after ΔT_c is exceeded is indicated by the fractional reduction in strength, $\sigma_i - \sigma_s/\sigma_i$, where σ_s is the as-shocked strength. It is usual in thermal shock experiments to find a region between ΔT_c and a higher critical temperature difference, $\Delta T_c'$, where the shocked strength remains constant [12]. This is not so in all the

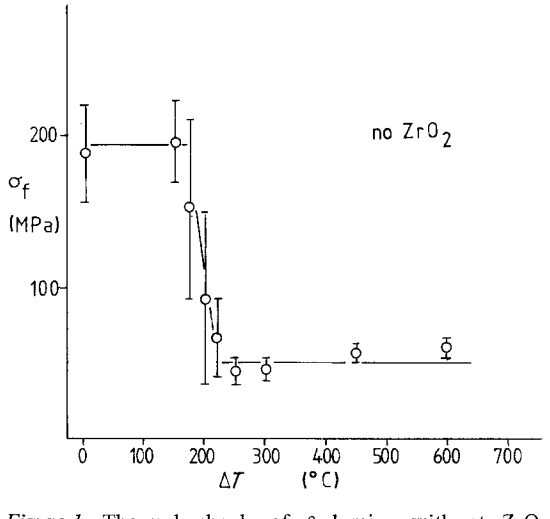

Figure 1 Thermal shock of β-alumina without ZrO_2 additions.

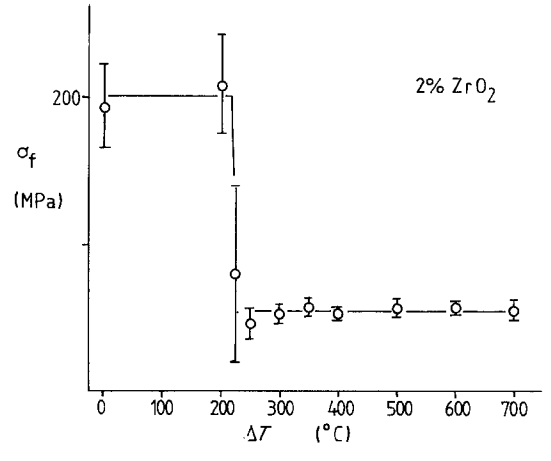

Figure 2 Thermal shock of β-alumina with 2% ZrO_2.

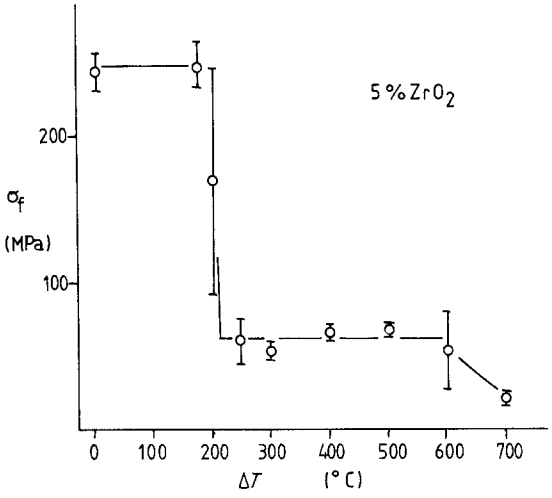

Figure 3 Thermal shock of β-alumina with 5% ZrO_2.

present results where visible maxima occur at $\Delta T \approx 500^\circ$ C for the 10% ZrO_2 material. Thus in Table IV two values are given for the fractional reduction in strength; that at 300° C which represents the damage just after ΔT_c is exceeded and at 500° C which is the minimum value of reduction in strength.

The considerable weakening just above ΔT_c appears to be associated with the small number of thermal shock cracks in this region of the curve (Table V). The available elastic energy is dissipated in a small number of critical cracks and below a certain microcrack density, corresponding in this case to ~15% ZrO_2, the microcrack method of absorbing energy appears not to function. At higher quench temperatures a large number of thermal shock cracks grow in a very short time and

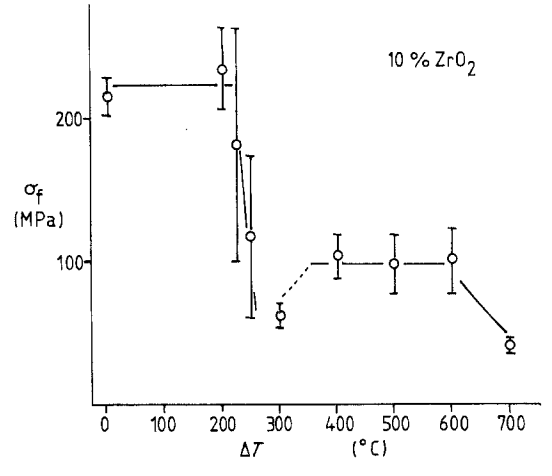

Figure 4 Thermal shock of β-alumina with 10% ZrO_2.

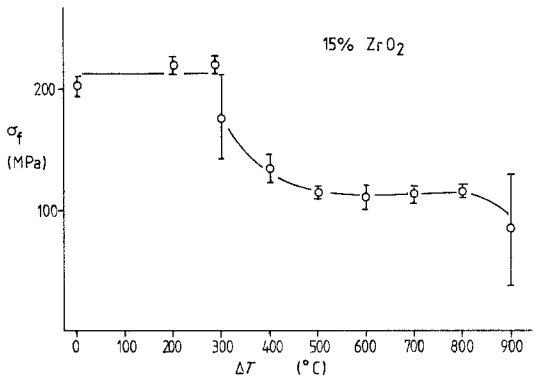

Figure 5 Thermal shock of β-alumina with 15% ZrO_2.

it is likely that crack arrest by bifurcation in the region of ZrO_2 particles operates [13]. At the 15% ZrO_2 level, however, the distribution of zirconia is sufficient to give a high density of microcracks and is able to arrest thermal shock cracks throughout the quenching range. A material with dramatically enhanced thermal shock resistance and damage resistance is produced, being able to retain 57% strength after a water quench from 800° C (Fig. 5).

3.2. Microscopy

Zirconia particles are easily distinguished from β-alumina matrix in scanning electron microscopy of polished sections with a minimum thickness of sputter-coated gold because of the enhanced back scattered electron contribution to the image. At the 2% ZrO_2 level the ZrO_2 particles did not exceed 0.5 μm and poor contrast was obtained (Fig. 7). At the 5% ZrO_2 level sufficient particle coarsening occurred to give ~4 μm particles which were clearly observable (Fig. 8). Although the

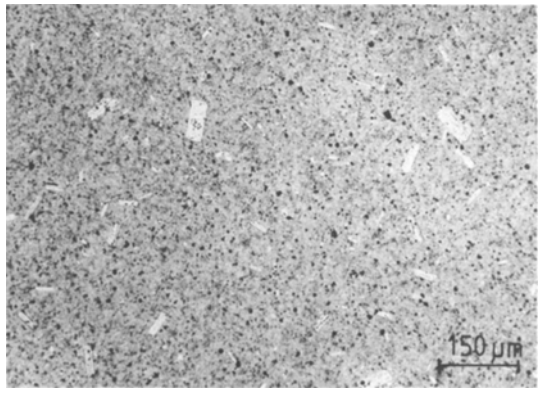

Figure 6 Optical micrograph thermally etched section of β-alumina, 15% ZrO_2.

TABLE IV Thermal shock characteristics of ZrO_2 toughened β-alumina

Wt % ZrO_2	Initial strength (MPa)	ΔT_c (° C)	$\Delta T = 300°$ C $\frac{\sigma_i - \sigma_s}{\sigma_i}$	$\Delta T = 500°$ C $\frac{\sigma_i - \sigma_s}{\sigma_i}$
0	192	195	0.76	0.69
2	193	205	0.73	0.70
5	244	200	0.77	0.71
10	216	225	0.71	0.54
15	202	300	0.12	0.43

chemical etching treatment tends to enhance polishing scratches by removing debris, it is essential for observation of the microcracking around large ZrO_2 particles (Figs. 8 to 10).

Figs. 11 and 12 show the extensive regions of crack bifurcation in the vicinity of a thermal shock crack. It is noteworthy that cracked zirconia particles were rarely observed; the crack often passed on both sides of a large undamaged particle.

The extent of disturbance to the polycrystal on either side of the thermal shock cracks was evident in the optical microscope (Fig. 13). From micrographs of this type it was possible to estimate the crack length per unit area for 10% ZrO_2 samples quenched from different temperatures and the value of this parameter, determined by quantitative image analysis, is shown in Table V. No thermal shock cracks were observed in samples taken from the 250° C quench (Fig. 4) illustrating the very small number of cracks actually present and the difficulty of sampling in the optical microscope.

Transmission electron microscopy shows the morphology of the coarsened ZrO_2 particles in more detail (Fig. 14). The dark ZrO_2 particle (centre) in this 15% ZrO_2 sample is typical of the unusual shapes observed. These appear to have coarsened by grain boundary transport in competition with the growing β-alumina grains. The twinning can be seen clearly. On the other hand ZrO_2 particles which have been trapped in a large β-alumina grain generally have rounded shapes (Fig. 15). It is likely that the unusual shapes of intergranular particles of ZrO_2 arise from arbitrary sections through larger and more spherical particles which contain or surround smaller β-alumina grains. Without such a structure it is difficult to see how coarsening mechanisms (in which material from fine grains is deposited on regions of lower curvature) can proceed.

By comparing micrographs of 2% and 5% ZrO_2 material the upper limit on particle size to retain tetragonal unalloyed ZrO_2 is estimated as $\approx 0.4\,\mu m$. Such a small value is partly attributable to the low elastic modulus of β-alumina (197 GPa) compared with ZrO_2 (207 GPa).

TABLE V Crack length per unit area for β-alumina–10% ZrO_2 quenched from various temperatures

ΔT (° C)	Crack length (m^{-1})
300	710
400	2530
500	3250
600	5770

4. Conclusions

The effect of making zirconia additions to β-alumina electrolytes by the sodium zirconate route has been investigated, with particular attention to initial strength and thermal shock. Zirconia particle coarsening takes place during the β-alumina sintering process and the resulting particle size is related to the amount of zirconia added. For 2% ZrO_2 the particles do not exceed $0.5\,\mu m$, for 15% ZrO_2 the particles grow to $\sim 12\,\mu m$. The larger particles have transformed to monoclinic on cooling and microcracks can be observed by scanning electron microscopy of polished sections after chemical etching. The microcracking mechanism has effected a reduction in strength of the finished article but an improvement in thermal shock resistance. The thermal shock strength–quenching temperature diagrams show an unusual maximum in strength in the region between ΔT_c and $\Delta T_c'$ which is not presently fully understood.

The damage resistance of material with 15% ZrO_2 is considerably improved. Scanning electron microscopy shows the wide regions of crack bifurcation in thermal shock fracture which are thought to demonstrate the main energy absorbing mechanism.

This study shows that the addition of zirconia by the sodium zirconate route, although expected

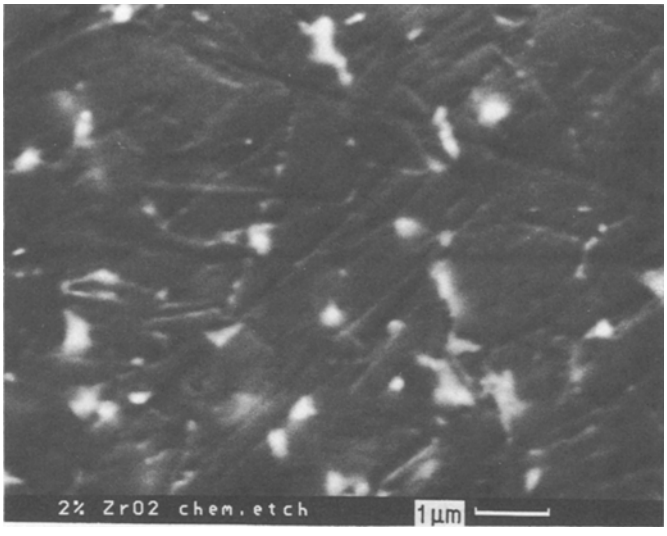

Figure 7 SEM chemically etched section β-alumina, 2% ZrO_2.

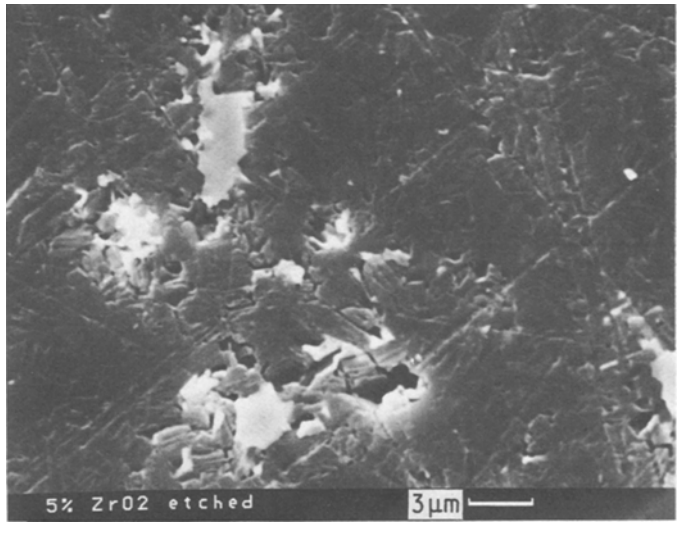

Figure 8 SEM chemically etched section β-alumina, 5% ZrO_2.

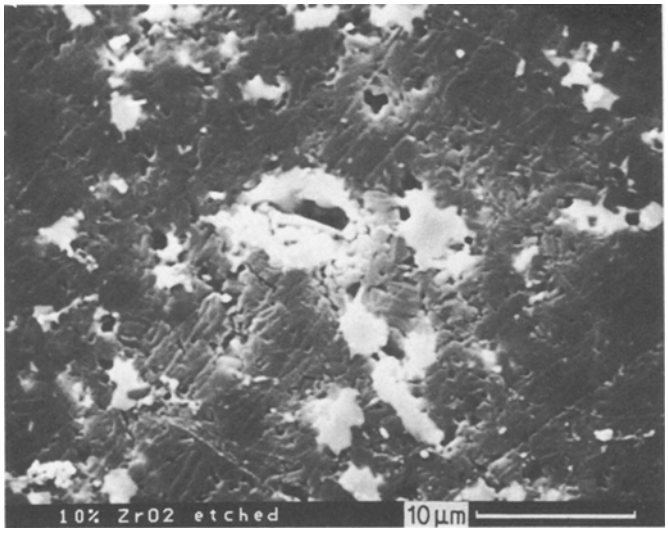

Figure 9 SEM chemically etched section β-alumina, 10% ZrO_2.

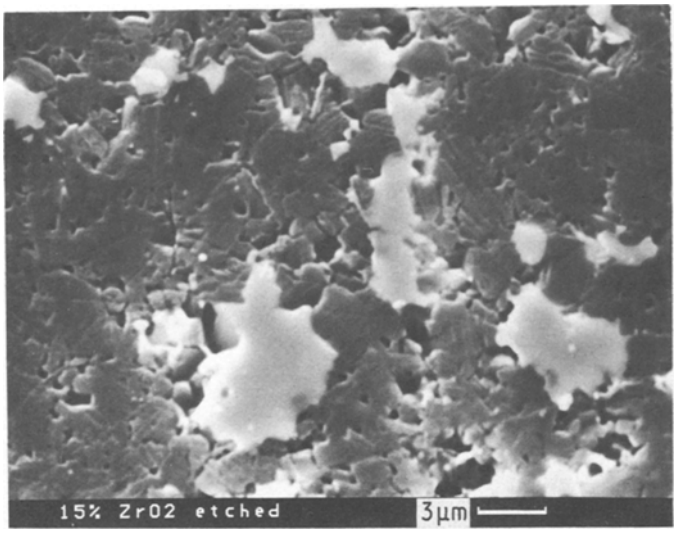

Figure 10 SEM chemically etched section 15% ZrO_2.

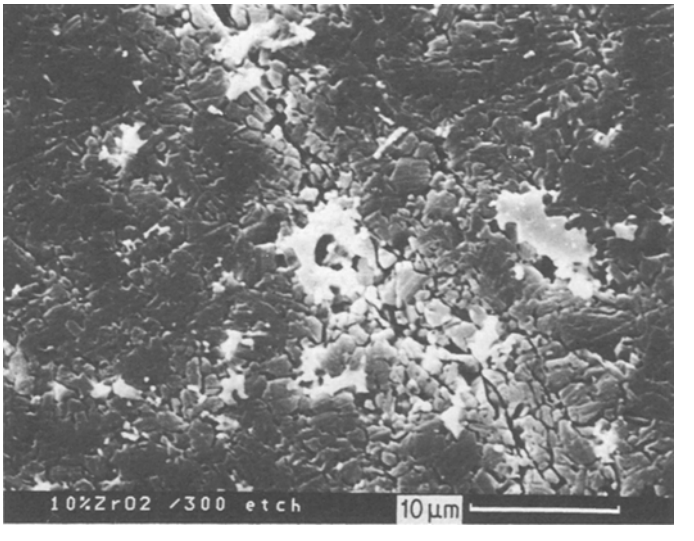

Figure 11 SEM chemically etched section 10% ZrO_2 quenched from 300° C.

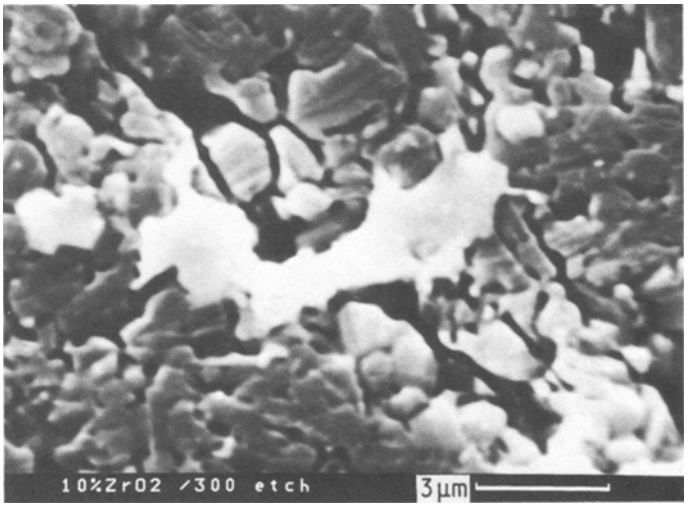

Figure 12 SEM chemically etched section 10% ZrO_2 quenched from 300° C.

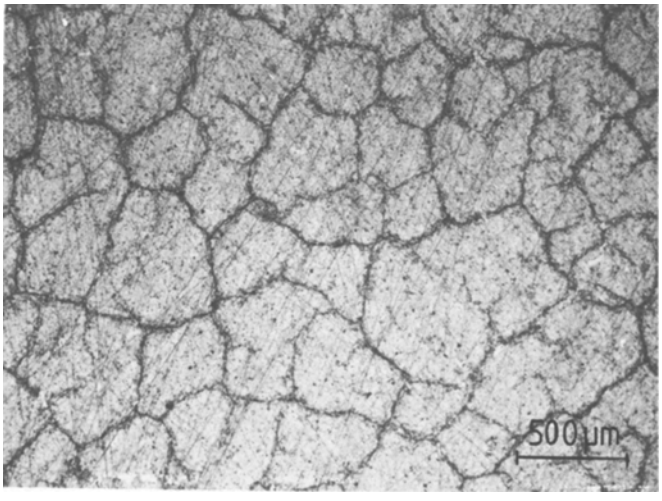

Figure 13 Optical micrograph 10% ZrO_2 $\Delta T = 600$.

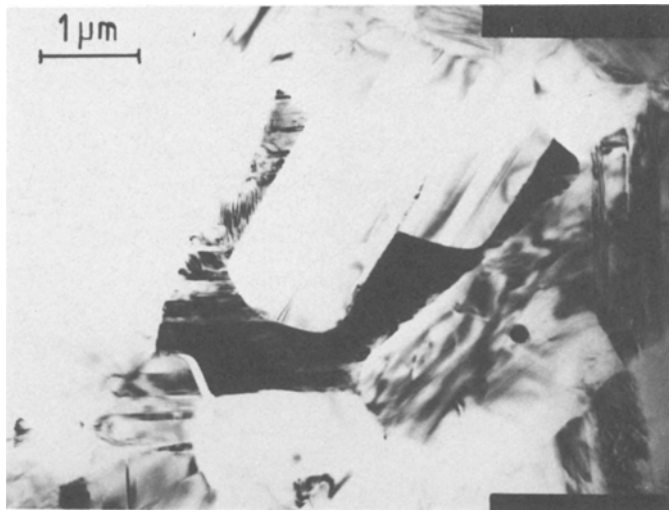

Figure 14 TEM β-alumina with 15% ZrO_2.

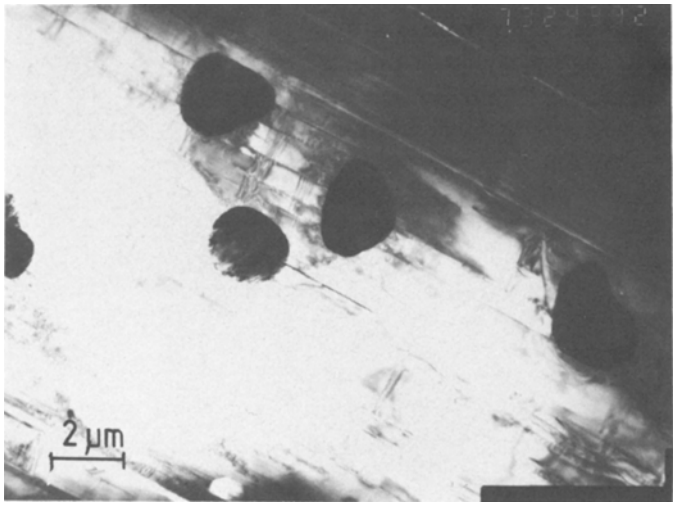

Figure 15 TEM β-alumina with 15% ZrO_2.

to produce a fine dispersion, is unsuitable for zirconia toughening of β-alumina intended for battery applications unless the coarsening process can be identified and controlled. However, it clearly demonstrates that a β-alumina with superior thermal shock resistance and damage resistance can be obtained by zirconia additions and this may be of use where β-alumina is used in, for example, refractory applications.

References

1. F. F. LANGE, *J. Mater. Sci.* 17 (1982) 235.
2. R. C. GARVIE, R. H. HANNICK and R. T. PASCOE, *Nature* 258 (1975) 703.
3. H. RUF and A. G. EVANS, *J. Amer. Ceram. Soc.* 66 (1983) 328.
4. L. VISWANATHAN, Y. IKUMA and A. V. VIRKAR, *J. Mater. Sci.* 18 (1983) 109.
5. F. F. LANGE, B. I. DAVIES and D. O. RALEIGH, *Comm. Amer. Ceram. Soc.* 66 (1983) C50.
6. J. R. G. EVANS, R. STEVENS and S. R. TAN, Submitted to *J. Mater. Sci.*
7. J. R. G. EVANS and R. STEVENS, *B. Ceram. Trans. J.* 83 (1984) 14.
8. Calculated from data by P. EVANS and R. STEVENS, to be published.
9. F. F. LANGE, *J. Mater. Sci.* 17 (1982) 225.
10. R. STEVENS, "Zirconia", MEL Monograph (1983).
11. W. D. KINGERY, *J. Amer. Ceram. Soc.* 38 (1955) 3.
12. D. P. H. HASSELMAN, *ibid.* 52 (1969) 600.
13. N. CLAUSSEN and D. P. H. HASSELMAN, "Thermal Stress in Severe Environments", edited by D. P. H. Hasselman and R. A. Heller (Plenum, New York, 1980).

Received 7 February
and accepted 29 February 1984